P-Polarized Reflectance Spectroscopy: A high sensitive real-time monitoring technique to study surface kinetics under steady state epitaxial deposition conditions

Nikolaus Dietz[a,b] and Klaus J. Bachmann[b,c]

Departments of Physics[a], Materials Science[b] and Chemical Engineering[c]

North Carolina State University, Raleigh, North Carolina 27695-7919

IN-25-CR
6065

p_31

Abstract

This paper describes the results of real-time optical monitoring of epitaxial growth processes by p-polarized reflectance spectroscopy (PRS) using a single wavelength application under pulsed chemical beam epitaxy (PCBE) condition. The high surface sensitivity of PRS allows the monitoring of submonolayer precursors coverage on the surface as shown for GaP homoepitaxy and GaP on Si heteroepitaxy as examples. In the case of heteroepitaxy, the growth rate and optical properties are revealed by PRS using interference oscillations as they occur during growth. Superimposed on these interference oscillations, the PRS signal exhibits a fine structure caused by the periodic alteration of the surface chemistry by the pulsed supply of chemical precursors. This fine structure is modeled under conditions where the surface chemistry cycles between phosphorus supersaturated and phosphorus depleted surfaces. The mathematical model describes the fine structure using a surface layer that increases during the tertiarybutyl phosphine (TBP) supply and decreases during and after the triethylgallium (TEG) pulse, which increases the growing GaP film thickness. The imaginary part of the dielectric function of the surface layer is revealed from the turning points in the fine structure, where the optical response to the first precursor pulse in the cycle sequence changes sign. The amplitude of the fine structure is determined by the surface layer thickness and the complex dielectric functions for the surface layer with the underlying bulk film. Surface kinetic data can be obtained by analyzing the rise and decay transients of the fine structure.

Introduction

The engineering of advanced microelectronic circuits, optoelectronic devices and integrated optical circuits requires precise control of the lateral dimensions and thicknesses of device features and structural perfection of heterostructures. The use of optical diagnostic techniques for the real-time monitoring of the deposition process is attractive due to their non-destructive character and their potential use for real-time feed-back control. A variety of optical real-time methods, such as such as kinetic reflectometry at both single[1] and multiple[2] wavelengths, pyrometric interferometry (PI)[3], spectral ellipsometry (SE), surface photo absorption (SPA)[4-6] and reflectance-difference spectroscopy (RDS)[7] were developed during the last decades demonstrating their applicability to a variety of deposition processes, monitoring film thickness and optical properties of the growing film, including in a few cases, real-time feed-back control[8]. In order to relate the surface chemistry and kinetics of the film growth to the precise control of the film properties, a real-time technique must combine high surface sensitivity with the capability to reveal film properties such as thickness and the dielectric function.

We recently introduced a real-time optical monitoring technique, p-polarized reflectance spectroscopy (PRS), which achieves both: (i) high sensitivity to surface chemistry processes and (ii) the monitoring of film thickness and optical properties with submonolayer resolution[9]. PRS is based on changes in the reflectance of p-polarized light that impinges the surface near the Brewster angle of the substrate (For an absorbing medium the generalized Brewster angle is also called pseudo-Brewster angle or first Brewster angle). The Brewster angle condition is chosen to suppress the substrate reflectance by three to four orders of magnitude, thereby achieving high surface sensitivity during the heteroepitaxial nucleation and overgrowth process. In contrast to SPA that probes an absorbent surface layer, PRS probes the differences between the complex dielectric functions of surface layer, film and/or substrate. An absorption in the surface layer or underlying film/substrate is included in the description, but not required. Using probe light energies in the transparent or weakly absorbing region of the deposited film, PRS uniquely probes both the film properties and simultaneously the properties of the surface layer with high sensitivity. This allows film thickness to be monitored by interference oscillations[10], the optical

dielectric function of the growing film to be evaluated by analyzing the differences in the dielectric function for the film and the substrate, and the surface chemistry and kinetics to be studied during the deposition process by analyzing the fine structure that is superimposed to the interference oscillation of the growing film[9,11-14]. The combined application of PRS and laser light scattering (LLS) for real-time optical monitoring of surface, interface and bulk properties provides additional insight into the kinetics and mechanism of deposition processes. Combining PRS and LLS allows evaluation and improvement of process conditions, such as surface preconditioning, deposition temperature, and V:III precursor ratio for the preparation of improved materials.

In this paper, we briefly summarize results obtained by PRS and LLS during the heteroepitaxial film growth of GaP on Si substrates, as well as the homoepitaxial growth of GaP epilayers and focusing afterwards on a more detailed description of the observed fine structure by introducing a simplified single surface layer model to describe the fine structure in terms of a periodic changed surface layer due to the pulsed precursor supply.

Experiment and Results

For single wavelength PRS and LLS we employed a p-polarized light beam generated by a HeNe laser (λ=6328Å) and a Glan-Thompson prism. The beam impinges on the substrate at an angle of incidence φ=72°. The angle of incidence can be adjusted in the range of 70°-75°and set with an accuracy of 0.01°. The reflected beam is detected by a Si photodiode. The intensity of the scattered radiation is monitored simultaneously by a photo multiplier tube (PMT) located 45° from the plane of incidence. Further details on the experimental conditions are given in a previous publication[9]. The experimental limitations of this technique due to depolarization and/or angular divergence are discussed in reference 10.

The fluxes of the gas sources TEG [Ga(C_2H_5)$_3$], TBP [(C_4H_9)PH$_2$] and hydrogen, are established by mass flow controllers and are directed via computer-controlled 3-way valves to either the reactor chamber or a separately pumped bypass chamber. This allows the sequential exposure of the substrate to individual pulses of the precursor molecules without overall pressure

variations. The overall pressure during the deposition lays in the order of 10^{-4} to 10^{-5} torr, whereby the major contribution (10^{-4} torr) is given by molecular hydrogen. An interaction of the gas species with the probe light in this pressure range can be neglected. The switching of the sources is synchronized with the data acquisition of the PRS and LLS signals to correlate changes in the reflected intensity to chemistry-induced changes in the surface conditioning and/or in the optical properties of the growing film.

Figure 1 shows the time-evolution of the PRS and LLS signals during the growth of GaP on Si(001) at 350°C with a precursor cycle sequence time of 7 sec. The evolution of the PRS and LLS signals during growth can be analyzed in terms of the bulk and surface properties of the film as summarized in table 1. In this paper we focus on the description and modeling of the fine structure in the PRS signal, which is superimposed on to the interference oscillation associated with the growing film. For a detailed discussion of the other features, we refer the reader to previous publications[9,11-16].

The fine structure observed in the PRS signal (not resolved in fig. 1) is strongly correlated to the time sequence of the supply of precursors employed during the steady-state growth of GaP. Figure 2 shows the fine structure and its correlation with the precursor pulse sequence as observed at the beginning in fig. 1. Each peak in the fine structure corresponds to a complete precursor cycle with the start of the oscillation always coinciding with the leading edge of the first TBP pulse of the sequence. Under the conditions shown in fig. 1 and 2, the fine structure oscillation is built up by a increasing reflectance during exposure to TBP and a decreasing reflectance after exposure to TEG. As it can be seen in fig. 1, the amplitude in the fine structure changes during deposition time. The amplitude increases on the raising flank of the interference oscillation with a maximum at the top, and then decreases on the falling flank. The relative locations of these decreases and increases in the fine structure amplitude and the film interference oscillation strongly depend on the chosen growth conditions, such as precursor pulse width and height, pulse sequence time, or supply of additional activated hydrogen. Figure 3 shows an example of the time evolution of the PRS signal using a 4 sec pulse cycle sequence (TBP form 0 - 0.8 sec and TEG from 1.4 - 1.8 sec) with a continuous flow of hydrogen and

thermally activated TBP and hydrogen. In this case, the fine structure decreases at the minima and maxima of the interference oscillations and increases at the raising and falling flanks. The inserts in fig. 3 show an enlargement at the interference minima. The start of each pulse cycle sequence in the inserts is indicated with a dashed line, where the distance between each dashed represent one pulse cycle sequence of 4 sec. The inserts show that the areas of minimum amplitude in the fine structure coincide with the extreme of the interference pattern. Also note, that the optical response to the first precursor pulse in each cycle sequence changes form a raising transient (begin of the insert) to a falling transient (end of the insert). This change-over in the sign with respect to the optical response of the first precursor pulse will be in the further text denoted as the turning point of the fine structure.

In the case of homoepitaxy, the interference oscillation due to the growing film does not appear, but the fine structure persists, as shown in fig. 4 for a GaP PCBE experiment. Curves (a), (b) and (c) in fig. 4 are the PRS traces during the deposition times of 0 to 600 sec, 600 to 1200 sec and 1200 - 1800 sec, respectively. Note that the modulation of the amplitude and baseline exhibits at least two frequencies in addition to the bimodal envelope modulation. The detailed appearance depends strongly on the chosen individual precursor exposure duration. Conditions exist for which the bimodal envelope exhibition vanishes and only a long term oscillations in the base line of the fine structure are observed. The bimodal envelope modulations during homoepitaxial growth are commensurate to the observed pattern under heteroepitaxial GaP on Si growth, allowing the calibrating of growth rates in the homoepitaxy using identical growth conditions for heteroepitaxy. The growth rate for this experiment is 3.1Å/cycle (±3%) with a precursor cycle sequence of 4 sec and a growth temperature of 350°C.

Some characteristic features in the evolution of the fine structure differ between homoepitaxial and heteroepitaxial growth conditions:

(i)   In the case of homoepitaxy, no turning point in the fine structure exist.

(ii)   In the bimodal envelope modulation of the fine structure, the height of the amplitude alternate in a ratio of 3:1 during homoepitaxial growth, whereas under heteroepitaxial growth condition, this ratio is about 2:1.

(iii) Under homoepitaxial growth conditions, an additional long term oscillation in the base line of the fine structure is observed with oscillation times of the order of 100 sec or more.

and

(iv) During homoepitaxial growth the periodicity in the fine structure is occasionally interrupted by a missing or strongly suppressed response to one precursor cycle sequence as can be seen on locations marked in fig. 4 with an arrow. The optical response to the cycle sequence afterwards is significantly reduced. This phenomenon is observed for different cycle sequences and growth conditions.

Fine Structure Modeling

In a first attempt to model the fine structure, we assume that the fine structure is caused by the presence of a periodically changed surface layer on top of the growing GaP film, which can be described by a four-layer (ambient / surface_layer / film / substrate) stack as schematically shown in figure 5. Fresnel's equations for a multilayer stack- as described previously[9] - are used to calculate the changes of the reflectivity for p-polarized light as a function of layer thickness, assuming homogenous isotropic media. Labeling the media forming the stack a for ambient, p for surface_layer, f for film, and s for substrate with the interfaces labeled ap, pf and fs, the complex reflectance amplitude rr_{apfs} for p-polarized light is given by

$$rr_{apfs} = \frac{r_{ap} + r_{pf}\, e^{-2j\Phi_p} + r_{fs}\, e^{-2j(\Phi_f + \Phi_p)} + r_{ap}\, r_{pf}\, r_{fs}\, e^{-2j\Phi_f}}{1 + r_{ap}\, r_{pf}\, e^{-2j\Phi_p} + r_{ap}\, r_{fs}\, e^{-2j(\Phi_p + \Phi_f)} + r_{pf}\, r_{fs}\, e^{-2j\Phi_f}} \qquad (1)$$

with the reflectance coefficients as a function of the complex dielectric constants ε

$$r_{ap} = \frac{\varepsilon_p \cos\varphi - \sqrt{\varepsilon_a} \sqrt{\varepsilon_p - \varepsilon_a \sin^2\varphi}}{\varepsilon_p \cos\varphi + \sqrt{\varepsilon_a} \sqrt{\varepsilon_p - \varepsilon_a \sin^2\varphi}} ,$$

$$r_{pf} = \frac{\varepsilon_f \sqrt{\varepsilon_p - \varepsilon_a \sin^2\varphi} - \varepsilon_p \sqrt{\varepsilon_f - \varepsilon_a \sin^2\varphi}}{\varepsilon_f \sqrt{\varepsilon_p - \varepsilon_a \sin^2\varphi} + \varepsilon_p \sqrt{\varepsilon_f - \varepsilon_a \sin^2\varphi}} , \qquad (2)$$

$$r_{fs} = \frac{\varepsilon_s \sqrt{\varepsilon_f - \varepsilon_a \sin^2\varphi} - \varepsilon_f \sqrt{\varepsilon_s - \varepsilon_a \sin^2\varphi}}{\varepsilon_s \sqrt{\varepsilon_f - \varepsilon_a \sin^2\varphi} + \varepsilon_f \sqrt{\varepsilon_s - \varepsilon_a \sin^2\varphi}}$$

and the phase factors

$$\Phi_p = \frac{2\pi d_p}{\lambda} \sqrt{\varepsilon_p - \varepsilon_a \sin^2\varphi} \quad \text{and} \quad \Phi_f = \frac{2\pi d_f}{\lambda} \sqrt{\varepsilon_f - \varepsilon_a \sin^2\varphi} . \qquad (3)$$

The fine structure in the PRS signal is modeled by a periodically increased and decreased surface layer and the GaP film growth by incorporation of the surface layer in the growing film. The precursor cycle sequence that describes the time dependent exposure of the surface to TBP and TEG is schematically shown in Figure 6. This cycle sequence is linked to the surface layer and its consumption during the growth of a GaP layer by the following simplified assumptions. During the exposure of the surface with TBP, an exponential increase of a surface layer $d_p(t)$ is assumed according to the equation

$$d_p(t) = \beta + \gamma \cdot \exp(\alpha_{tbp} \cdot t); \qquad (b\_{tbp} \le t \le e\_{tbp}) \qquad (4)$$

where β and γ,

$$\beta = -d_{cov} \Big/ \Big(\exp[\alpha_{tbp} \cdot (e\_{tbp} - b\_{tbp})] - 1 \Big)$$

$$\qquad (4b)$$

$$\gamma = d_{cov} \Big/ \Big(\exp(\alpha_{tbp} \cdot e\_{tbp}) - epx(\alpha_{tbp} \cdot b\_{tbp}) \Big)$$

are determined by the boundary conditions,

$$d_p(t = b\_{tbp}) = 0 \quad \text{and} \quad d_p(t = e\_{tbp}) = d_{cov} \qquad (4c)$$

d_{cov} denotes the thickness of the surface layer and α_{tbp} describes the build up of the surface layer, which is generally a function of flux profile, flux intensity, sticking coefficient and activation rates of the formed surface species contributing to the surface layer .

The exponential decay function that describes the consumption of the surface layer during its incorporation in the growing bulk film can be written as

$$d_p(t) = b + g \cdot \exp(-\alpha_{teg} \cdot t); \qquad (b_{\_teg} \leq t \leq e_{\_fil}) \qquad (5a)$$

with b and g

$$b = -d_{cov} \Big/ \Big(\exp[\,\alpha_{teg} \cdot (e_{\_fil} - b_{\_teg})\,] - 1 \Big)$$

$$g = d_{cov} \Big/ \Big(\exp(\alpha_{teg} \cdot b_{\_teg}) - epx(\alpha_{teg} \cdot e_{\_fil}) \Big) \qquad (5b)$$

and the boundary conditions

$$d_p(t = b_{\_teg}) = d_{cov} \quad \text{and} \quad d_p(t = e_{\_fil}) = 0 \qquad (5c)$$

as illustrated in fig. 6.

The increase of the bulk film is assumed to be directly linked to the incorporation of the surface layer in the bulk film by

$$\Delta d_{GaP}(t) = grocyc \cdot \frac{[\,d_{cov} - d_p(t)\,]}{d_{cov}}; \qquad (b_{\_teg} \leq t \leq e_{\_fil}) \qquad (6)$$

where grocyc denotes the growth rate per cycle sequence in Å. The decay parameter α_{teg} describes the TEG flux profile, the sticking coefficients of the TEG radicals as well as the chemical reaction rates transforming the surface species into GaP.

With these assumptions, the changes in the reflectivity are calculated by the time evolution of the top layer $d_p(t)$ {eqn. (4a) and (5a)} and by the GaP film thickness through $d_{GaP}(t) = N \cdot grocyc + \Delta d_{GaP}(t)$; (N = cycle sequence number). Figure 7 shows the temporal evolution of the surface layer, the increase in the bulk film thickness and the related changes in the reflectivity during several cycle sequences. The precursor cycle sequence, shown in fig. 7(a), consists of a TBP pulse from 0.0-0.8 sec and a TEG pulse from 1.4-1.7 sec and a total cycle time of 4 sec. Figure 7(b) shows the calculated changes in the thickness of the surface layer for a maximal surface coverage of $d_{cov} = 3\text{Å}$ and a complex dielectric function for the surface layer of $\varepsilon_p = (8.0, 2.0)$. The exponential increase of the surface layer is set to $a_{tbp} = 1.0$ and the decay factor α_{teg} describing the decrease of the surface layer is set to 2.0. The time-dependent increase of the bulk film thickness during the cycle sequence is shown in fig. 7(c) for

a growth rate of 3 Å per cycle. Curve (d) shows the calculated changes in the reflectivity during the time-evolution of the surface layer and the bulk film growth process with λ = 6328Å, angle of incidence φ = 72°, a complex dielectric function for the Si substrate of ε_{Si} = (15.25, 0.17)[17] and a complex dielectric function for the GaP bulk film of ε_{GaP} = (11.11, 0.0)[18].

For all further model calculations following parameters were kept constant, unless otherwise posted:

complex dielectric function for the substrate of ε_{Si} = (15.25, 0.17),

complex dielectric function for the bulk film of ε_{GaP} = (11.11, 0.0),

wavelength λ = 6328Å ,

cycle sequence 4 sec, with a TBP pulse from 0-0.8 sec, a TEG pulse from 1.4-1.8 sec

surface layer increase factor a_{tbp} = 1.0, surface layer decay factor a_{teg} =2.0;

a surface coverage of d_{cov} = 3Å

and

growth rate per cycle sequence 4Å/cycle.

With the cycle sequence of 4 sec and a growth rate of 4Å/cycle, the time scaling for the following presented figures can be 1:1 transformed into a thickness scale for a growing GaP film.

Figure 8 shows the time evolution of the PRS signal during the growth of a bulk film as a function of the imaginary part of the dielectric function ε_{p2} and a real part of the dielectric function ε_p = 6.0 of the surface layer. A well pronounced fine structure superimposed on the interference oscillation is observed in all cases, even without an assumed absorption in the surface layer, ε_{p2} =0. With an increasing absorption ε_{p2} =4, 8 and 12, in the surface layer, the amplitude in the fine structure increases. For ε_{p2} =0, the minimum amplitude of the fine structure occurs at the minima and maxima of the interference oscillations. The positions at which where the amplitude of these fine structure oscillations vanishes shifts towards lower film thicknesses with increased absorption in the surface layer. In fig. 9, we show an enlargement of this area of reduced fine structure amplitude. The position marked with an arrow indicates the position where

the optical response to the first TBP pulse in the cycle sequence changes sign. These turning points are shifted towards smaller times / smaller film thicknesses with greater absorption, allowing a highly accurate measurement of the absorptivity of the surface layer.

These simulated results are in excellent agreement with the experimental data shown in the inserts in fig. 3. Figure 10 shows a comparison of the experimental results, in the region of the turning point shown fig. 3, with calculated data assuming a surface coverage of 3Å and a growth rate of 3Å/cycle as determined from the interference oscillation of the growing film. To explain these data, the imaginary part of the dielectric function of the surface layer, ε_{p2}, must be zero because the turning point occurs at the minimum of the GaP interference oscillation. For ε_{p1} no unique information is available because the amplitude of the fine structure is a function of both the thickness of the surface layer and ε_{p1}. However, some conclusions regarding ε_{p1} can be drawn. For ε_{p1} greater than the dielectric function for the bulk film ε_{GaP}, the turning points in the fine structure are shifted towards higher film thickness with increasing absorption. This allows a qualitative assessment of ε_{p1} with respect to the underlying film.

Figure 11 shows the interference oscillation and the superimposed fine structure as a function of the angle of incidence φ near the Brewster angle of the substrate. The complex dielectric function of the surface layer is chosen to be $\varepsilon_p = (6.0, 4.0)$. The sequence for various angles of incidence shows that the sensitivity with respect to the surface layer induced fine structure remains even for a few degrees off the Brewster angle of the substrate. For one characteristic angle of incidence $\varphi = 73.3°$, the Brewster angle of the GaP film, the interference oscillation caused by the growing GaP film vanishes. At this angle, the fine structure and the turning points in the fine structure remain. This phenomenon can be used to determine independently the real part of dielectric function of the film and to gain high sensitivity to surface chemistry processes. At the same time, information is still available about the growth of the GaP film, which can be extracted from the turning points in the fine structure. The simulations show that these turning points do not occur during homoepitaxial growth, which is consistent with our experimental data. However, small deviations in optical properties of the growing homoepitaxial layer will result in an interference oscillation with an amplitude that is proportional to the deviations.

In order to simplify the expression for the reflectance as a function of surface layer thickness and ε_p, McIntyre and Aspnes[19,20] discussed theoretically the change in the reflectance, $\Delta R/R = (R_{afs} - R_{as})/R_{as}$, for thin surface layer (thickness $d_p \ll \lambda$) using a linear approximation in the phase factor Φ_f for a three layer (ambient/film/substrate) stack. This approximation is also used by Horikoshi et al.[21] and Hingerl et al.[22] to calculate the changes in $\Delta R/R$ under SPA conditions. Applying the linear approximation

$$e^{-2j\Phi_p} \approx 1 - 2j\Phi_p \tag{7}$$

to the four layer stack description, the approximate change in the reflectance for p-polarized light can be expressed by

$$\frac{\Delta R}{R} = \frac{R_{apfs^-} - R_{afs}}{R_{afs}} \tag{8}$$

where $R_{apfs^-} = rr_{apfs^-} \cdot rr_{apfs^-}{}^*$ denotes the approximate reflectance in a four layer stack, with the approximate reflectance coefficient

$$rr_{apsf^-} = \frac{r_{ap}\,r_{pf}\,(1-2j\Phi_p) + r_{fs}\,(1-2j\Phi_p)\,e^{-2j\Phi_f} + r_{ap}\,r_{pf}\,r_{fs}\,e^{-2j\Phi_f}}{1 + r_{ap}\,r_{pf}\,(1-2j\Phi_p) + r_{ap}\,r_{fs}\,(1-2j\Phi_p)\,e^{-2j\Phi_f} + r_{pf}\,r_{fs}\,e^{-2j\Phi_f}}. \tag{9}$$

R_{afs} denotes the reflectance for a three layer stack, ambient / film / substrate.

Figure 12(a) shows the calculate reflectance R_{apfs} and the reflectance R_{afs} without surface layer using the analytical Fresnel equations, for an angle of incidence of 72° and a transparent surface layer with $d_{cov} = 3\text{Å}$ and $\varepsilon_p = (6.0, 0.0)$. The resulting $\Delta R/R$, shown in fig. 12(b), contains two distinct features: (i) a modulation of the base line, where the maxima and minima in the baseline coincide in inverted order with the maxima and minima in the interference oscillations and (ii) an envelope modulation of the fine structure, where the turning points in the fine structure mark the minima and maxima positions in the baseline. Applying the linear surface layer approximation theory [equ. (9)] result in an error that is defined by

$$error(\%) = 100 \cdot \frac{\sqrt{\left(\frac{\Delta R^-}{R} - \frac{\Delta R}{R}\right)^2}}{\sqrt{\left(\frac{\Delta R}{R}\right)^2}} = 100 \cdot \sqrt{\frac{\left(R_{apfs^-} - R_{apfs}\right)^2}{\left(R_{apfs} - R_{afs}\right)^2}}. \tag{10}$$

This error exceeds 20% in the vicinity of the turning points of the fine structure. It strongly depends on the angle of incidence and the absorptivity of substrate and/or film. For the dielectric functions used in our calculations, a substantial error occurs in the angular range $65° \leq \phi \leq 75°$, close to the Brewster angle of the substrate. Under homoepitaxial growth conditions, where this approximation is applied to a three layer stack (ambient / surface layer / substrate), a significant error due to the linear approximation occurs in the whole angular range, except at the Brewster angle itself, where the error is zero. For strongly absorbing films and substrates, as used in the calculations by McIntyre and Aspnes[19], the error is typically below 2% in the angular range from $0 \leq \phi \leq 70°$. Above 70°, the error increases and has a maximum in the limit $\Delta R/R \approx 0$. Since PRS operates close to the Brewster angle and applies also to weakly and non-absorbing media, the linear approximation of ref. 19 cannot be used in order to simplify the analytical equations for the reflectance as a function of surface layer thickness and ε_p.

The sensitivity of the shift of the turning point, Δ_t, in the fine structure during GaP heteroepitaxy on a silicon substrate is shown in fig. 13, where the normalized shift relative to a chosen minimum in the interference oscillation is plotted as a function of ε_{p2} for various values of ε_{p1}. In this calculation Δ_t increases with increasing absorption, while the resolution decreases for higher ε_{p2} values. The accuracy to which ε_{p2} can be resolved depends also on the difference $\Delta_{p-1} = |\varepsilon_{p1} - \varepsilon_{GaP1}|$. For $\Delta_{p-1} > 4$ Δ_t is nearly linear in ε_{p2} ($\varepsilon_{p2} < 12$). The error associated with ε_{p2} is then given by the accuracy of the determination of the turning point in the fine structure with respect to the minimum in the interference oscillation. This can be done within the accuracy of one precursor cycle sequence corresponding to 4-5Å film growth under typical growth conditions used for GaP heteroepitaxy on Si (see fig. 13 for an evaluation of the error). For $0 < \Delta_{p-1} < 4$ the resolution in the determination of ε_{p2} increases for smaller ε_{p2} values, approaching the highest sensitivity for small ε_{p2} values, that is, when Δ_{p-1} becomes close to zero. $\Delta_{p-1} = 0$ represents homoepitaxial growth conditions, for which the turning point in the fine structure vanishes.

The experimental capability of PRS to resolve the surface-layer-induced fine structure with high resolution and accuracy during the GaP growth under PCBE conditions allows a detailed

study of surface chemistry and kinetics. Figure 13 shows the changes in the falling transient of the fine structure varying the decay factor α_{teg} from 0.5 to 4.0. A line form analysis should allow to extract data such as the time constant of the overall reaction rate and - in connection with other independent input parameter, for example mass spectrometric data, an insight in the reaction mechanism.

Conclusion

PRS uniquely combines highly sensitive real-time optical monitoring of surface processes with the monitoring of film properties. The first attempt at modeling the surface chemistry that is provided in this paper describes the overall chemical changes at the surface in terms of the associated changes in the dielectric function of a single surface layer that alters thickness periodically. This explains the occurrence of the fine structure and the turning points in the fine structure as a function of the optical properties of the surface layer with respect to the underlying film and substrate during heteroepitaxial growth. The model, which is based on a four layer stack (ambient / surface layer / film / substrate), shows that no surface photo absorption is required in order to observe this fine structure. The positions of the turning point in the fine structure with respect to the minima and maxima are a direct measure for the absorptivity of the surface layer. The amplitude of the fine structure contains the thickness of the surface layer and differences in the dielectric functions of surface layer, underlying bulk film and substrate. A precise analysis of the fine structure line form in conjunction with supplementing analytical techniques allows the study of the surface chemistry and kinetics, gaining better understanding of precursor decomposition and surface activation rates as they affect the build up and incorporation of the surface species in the growing GaP film.

Acknowledgment

References

[1] J.V. Armstrong, T. Farrell, T.B. Joyce, P. Kightley, T.J. Bullough and P.J. Goodhew, J. Crystal Growth **120**, 84-87 (1992).

[2] K. P. Killeen and W. G. Breiland, J. Electronic Materials, **23**(2), 179-183 (1993).

[3] H. Grothe, F.G. Boebel, J. Crystal Growth, **127**, 1010-1013 (1993).

[4] H. Zama, K. Sakai and S. Oda, Jpn. J. Appl. Phys. Part 2 **31**(9A), L1243-5 (1992).

[5] N. Kobayashi, T. Makimoto, Y. Yamauchi and Y. Horikoshi, J. Cryst. Growth **107**(1-4), 62-7 (1991).

[6] T. Makimoto, Y. Yamauchi, N. Kobayashi and Y. Horikoshi, Jpn. J. Appl. Phys. **29**(2), L207-9 (1990).

[7] D. E. Aspnes, R. Bhat, E. Colas, V. G. Keramidas, M. A. Koza and A. A. Studna, J. Vac. Sci. & Technol. A **7**(3), 711-16 (1989).

[8] D. E. Aspnes, W. E. Quinn, M. C. Tamargo, M. A. A. Pudensi, S. A. Schwarz, M. J. S. P. Brasil, R. E. Nahory and S. Gregory, Appl. Phys. Lett. **60**(10), 1244 (1992).

[9] N. Dietz and K.J. Bachmann, MRS Bulletin **20**(5), p. 49-55 (1995).

[10] N. Dietz and H.J. Lewerenz, Appl. Surf. Sci. **69**, 350-354 (1993).

[11] K.J. Bachmann, U. Rossow and N. Dietz, Mater. Sci. & Eng. B, in press (1995).

[12] N. Dietz, U. Rossow, D. Aspnes and K.J. Bachmann, J. Elect. Mat., accepcted (1995).

[13] N. Dietz, A.E. Miller and K.J. Bachmann, J. Vac. Sci. Technol. A **13**(1), 153 (1995).

[14] N. Dietz, A.E. Miller, J.T. Kelliher, D. Venables and K.J. Bachmann, J. Cryst. Growth **150** 691-695 (1995).

[15] K.J. Bachmann, N. Dietz, A.E. Miller, D. Venables and J.T. Kelliher, J. Vac. Sci. Technol. A **13**(3), 696-704 (1995).

[16] A.E. Miller, J.T. Kelliher, N. Dietz and K.J. Bachmann, Mat. Res. Soc. Symp. Proc. **355**, Pittsburgh, in press (1995).

[17] D. F. Edwards, in Handbook of Optical Constants, ed. by E. D. Palik (Academic Press, 1985) 547 (1985).

[18] A. Borghesi and G. Guizzetti, in Handbook of Optical Constants, ed. by E. D. Palik (Academic Press, 1985) 445 (1985).

[19] J.D.E. McIntyre and D. E. Aspnes, Surface Science **24**, 417-434 (1971).

[20] J.D.E. McIntyre, in Optical Properties of Solids New Developments, ed, B.O. Serophin (North Holland Publishing Company) p. 556-630 (1971).

[21] Y. Horikoshi, J. Cryst. Growth **111**, 200 (1991).

[22] K. Hingerl, D.E. Aspnes and I. Kamiya, Surface Science **287/288**, 686 (1993).

Table 1:   Characteristic Features in the PRS and LLS signals and related information

Observed feature	Related information
Changes in the reflected intensity during heat-up	Temperature dependence of the dielectric function of the substrate and surface conditioning
Spacing in the minima/maxima of the film interference oscillation	Growth rate
Amplitude of film interference oscillation	Dielectric function of film
Initial nucleation period	Growth mechanism
Fine structure oscillations	Surface chemistry and kinetics
Locations of turing points of the fine structure with respect to the minima/maxima of the interference oscillations	Imaginary part of the dielectric function of the surface layer
Bimodal envelope modulation of the fine structure	Surface reconstruction
Evolution of scattered light	Surface roughening / Interface perfection / Defect formation

Figure Captions

Figure 1:   Experimental result: Interference oscillations in GaP on Si heteroepitaxy

Figure 2:   Correlation of fine structure in the PRS signal and timing sequence of the precursor pluses.

Figure 3:   Turning point of fine structure oscillation. The dased lines in the insert represent always the begin of a new pulse cycle sequence. Each pulse cycle sequence has a duration of 4 sec an is build up by a TBP pulse followed by a pause, a TEG pluse and a second pause (see text).

Figure 4:   Time-evolution of the PRS signal during GaP homoepitaxy.

Figure 5:   Schematic representation of a four layer stack

Figure 6:   Schematic model description for the time evolution of the surface layer and the bulk film growth

Figure 7:   (a) Precursor cycle sequence with a TBP pulse from 0.0-0.8 sec and a TEG pulse from 1.4-1.8 sec; (b) calculated changes in the thickness of the surface layer; (c) time-dependent increase of the bulk film thickness during the cycle sequence with a growth rate of 3 Å per cycle and (d) calculated changes in the reflectivity during the time-evolution of the surface layer and the bulk film growth process.

Figure 8:   Influence of the imaginary part of the dielectric function of the surface layer with a real part of the dielectric function of $\varepsilon_{p1} = 6.0$, which is smaller than the complex dielectric function for the bulk film of ε_{GaP}.

Figure 9:   Shift in the turning point of the superimposed interference due to the absorptivity in the surface layer with $\varepsilon_{p1} = 6.0$.
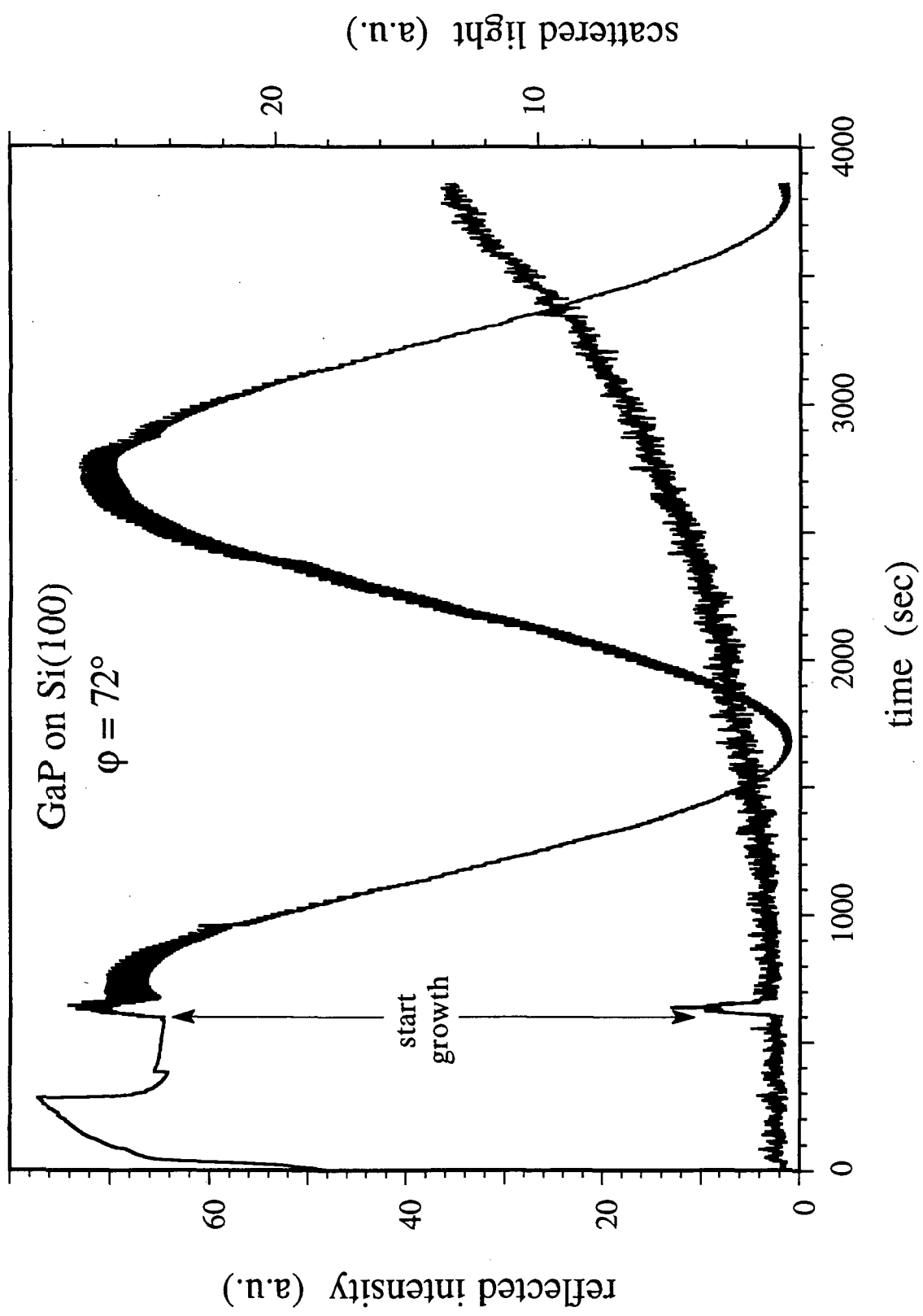
Figure 10: Comparison of experimental result for GaP heteroepitaxy on Si(100) at the turning point of the superimposed surface layer interference. The growth rate is 3Å/cycle and the angle of incidence is 72°. For the simulation we assumed a surface coverage of 3Å.

Figure 11: Influence of the chosen angle of incidence φ close to the Brewster angle of the substrate with $\varepsilon_p = (6.0, 4.0)$.

Figure 12: (a) Evolution of the reflectance during the growth with (lower trace) and without (upper trace) an additional transparent surface layer of 3Å with $\varepsilon_p = (6.0, 0.0)$; (b) calculated changes $\Delta R/R$ due to a present surface layer of 3Å; and (c) calculated error as it occur when a linear approximation is used for the description of the surface layer (see text).

Figure 13: Relative shift of the turning point Δ_t in the fine structure with respect to a minima in the interference oscillation during GaP heteroepitaxy on a silicon substrate. Shown are iso-terms of constant ε_{p1} as a function of ε_{p2}, for ε_{p1} values lower and higher than $\varepsilon_{GaP1} = 11.11$.

Figure 14: Changes in the falling transient of the fine structure by varying the decay factor α_{teg} from 0.5 to 4.0 with $\alpha_{tbp} = 1$, surface cover $d_{cov} = 3$Å, angle of incidence $\varphi=72°$ and $\varepsilon_p = (8.0, 2.0)$.

scattered light (a.u.)

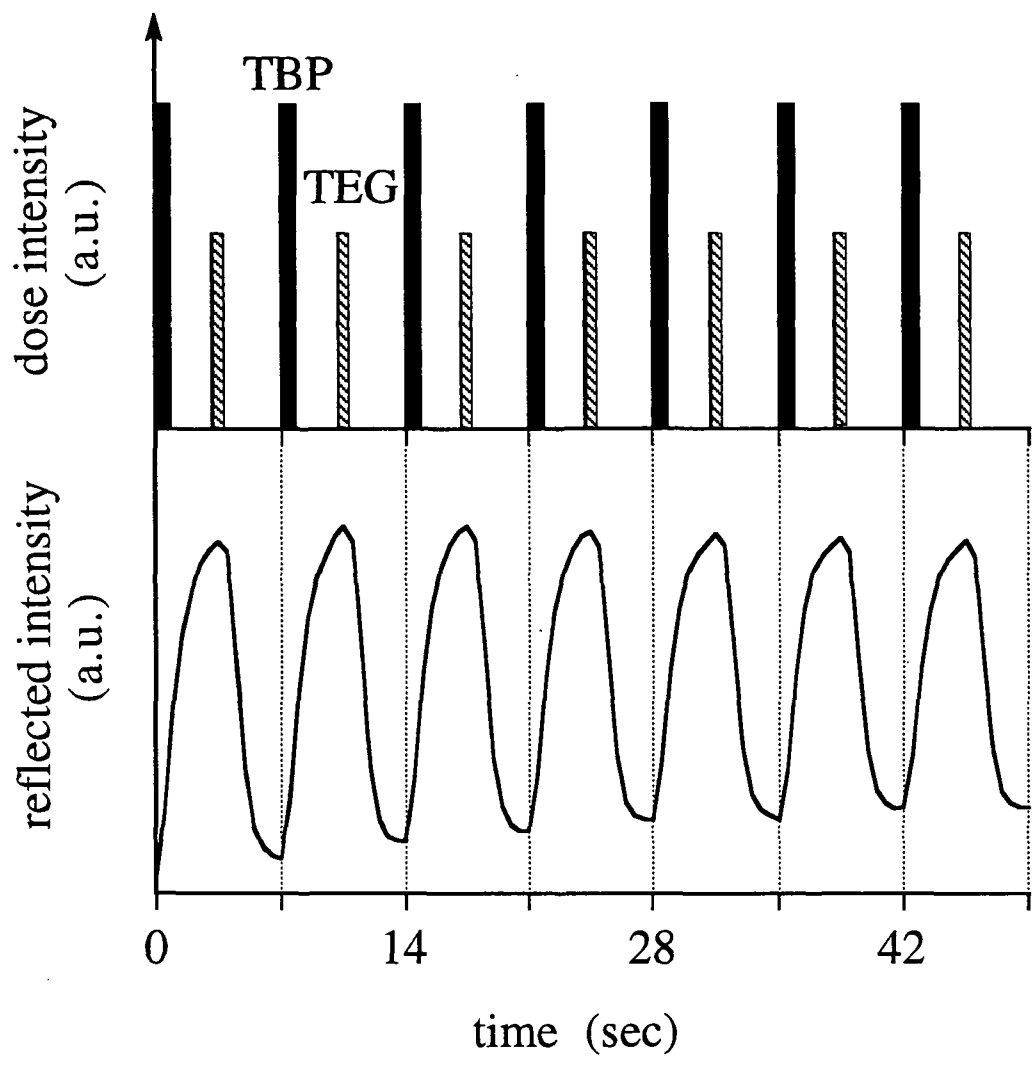reflected intensity (a.u.)

time (sec)

GaP on Si(100)
φ = 72°

start growth

Fig ①

fig ②

fig ③

reflected intensity (a.u.)

time (sec)

(a)

(b)

(c)

fig 4

ambient: ε_a

r_{ap}

surface layer: ε_p

r_{pf}

d_p

film: ε_f

r_{fs}

d_f

substrate: ε_s

φ

fig 5

fig 6

(a) flux (a.u.)
TBP
TEG

(b) surface coverage (Å)
3.0
0.0

(c) GaP film thickness (Å)
9.0
3.0

(d) reflected intensity (10^{+3} x R_p)
11.95
11.85

time (sec)
0   4   8   12   16

$\varepsilon_{p2} = 12$

$\varepsilon_{p2} = 8$

$\varepsilon_{p2} = 4$

$\varepsilon_{p2} = 0$

time (sec)

reflected intensity (10^{+3} x R_p)

11.0

8.0

5.0

0

500

1000

1500

fig ⑧

reflected intensity (10^{+3} x R_p)

time (sec)

$\varepsilon_{p2} = 12$

$\varepsilon_{p2} = 8$

$\varepsilon_{p2} = 4$

$\varepsilon_{p2} = 0$

fig 9

Experiment & Simulation

$\varepsilon_p = (8 / 0)$

$\varepsilon_p = (6 / 0)$

$\varepsilon_p = (4 / 0)$

Experiment GaP on Si

reflected intensity (a.u.)

0.35

0.25

0.15

time (sec)

100

116

132

fig 10

φ= 75°

φ= 74°

φ= 73.3°

φ= 73°

φ= 72°

reflected intensity $(10^{+3}$ x $R_p)$

time (sec)

14.0

10.0

6.0

2.0

0

500

1000

1500

Fig 11

(c) linear approximation error (%)

(b) $10^{+2} \, \Delta R / R$

(a) $10^{+3} \, R$

R_{afs}

R_{apfs}

time (sec)

fig ⑫

fig 13

Fig 14